Available online at www.sciencedirect.com
ScienceDirect
Journal of Catalysis 250 (2007) 94–101
JOURNAL OF CATALYSIS
www.elsevier.com/locate/jcat

Influence of gold particle size on the aqueous-phase oxidation of carbon monoxide and glycerol

William C. Ketchie [a], Yu-Lun Fang [b], Michael S. Wong [b], Mitsuhiro Murayama [c], Robert J. Davis [a,*]

[a] Department of Chemical Engineering, University of Virginia, 102 Engineers' Way, P.O. Box 400741, Charlottesville, VA 22904-4741, USA
[b] Department of Chemical and Biomolecular Engineering, Rice University, MS-362, 6100 Main Street, Houston, TX 77005-1892, USA
[c] Department of Materials Science and Engineering, University of Virginia, 116 Engineers' Way, P.O. Box 400745, Charlottesville, VA 22904-4745, USA

Received 1 May 2007; revised 31 May 2007; accepted 1 June 2007

Available online 29 June 2007

Abstract

Carbon-supported Au particles with mean sizes ranging from 5 to 42 nm and unsupported Au powder were evaluated as catalysts in the aqueous-phase oxidation of CO and glycerol. For the aqueous-phase oxidation of CO at pH 14 and 300 K, the turnover frequency (TOF) for the 5-nm Au particles was 5 s^{-1}, whereas the TOF for large supported Au (42 nm) and bulk Au were only 0.5 and 0.4 s^{-1}, respectively. The observed rate of peroxide formation during CO oxidation also was much higher on the small Au particles. Oxidation of glycerol in the aqueous phase at 333 K and elevated pH over the same catalysts revealed a similar influence of particle size, with the 5-nm Au particles giving a TOF of 17 s^{-1} at pH 13.8 and the larger particles and bulk Au nearly an order of magnitude less active. However, large Au particles (>20 nm) were more selective to glyceric acid. The lower selectivity of small Au particles is attributed to a higher formation rate of H_2O_2 during glycerol oxidation, because peroxide promotes C–C cleavage reaction.
© 2007 Elsevier Inc. All rights reserved.

Keywords: Gold; Oxidation; Carbon monoxide; Glycerol; Hydrogen peroxide; Aqueous; Hydroxyl; Glyceric acid; Glycolic acid; Particle size

1. Introduction

Catalysis by gold remains an area of intense interest as described in the recent review by Hashmi and Hutchings [1] and in the book by Bond et al. [2]. Although Au is quite a versatile catalyst, many unanswered questions remain concerning the active Au species during reaction. For example, there is still not a generally accepted mechanism for the low-temperature oxidation of CO. Nevertheless, the consensus regarding the vapor-phase oxidation of CO is that oxide-supported Au particles in the 2–4 nm size range are the most active [2]. Addition of water vapor to the CO oxidation reaction sometimes can increase the rate substantially, presumably due to the presence of hydroxyl groups on the surface [3–6]. Much less work has been performed on CO oxidation in the liquid phase. The Dumesic group studied the oxidation of CO by polyoxometalates and O_2 in the aqueous phase over Au nanotubes and found that increasing the hydroxyl concentration from pH 7 to 13 increased the oxidation rate by a factor of five [7–10]. Our research group observed that carbon-supported Au catalysts, which were inactive for the vapor-phase oxidation of CO up to 373 K, showed excellent CO oxidation rates in the aqueous phase at 300 K. Moreover, a 50-fold increase in rate was observed on going from acidic to basic pH [11]. The Au nanotubes and carbon-supported Au particles used in those aqueous-phase studies were larger than 4 nm [7–11].

During the aqueous-phase oxidation of diols, Prati and Rossi found that supported Au catalysts were active and selective for oxidation of the primary alcohol [12]. Subsequently, a number of researchers began investigating the oxidation of glycerol over Au catalysts in the aqueous phase [11,13–15]. This reaction is of interest because glycerol is a byproduct of biodiesel synthesis from triglyceride feedstocks. Biodiesel production rates in the US alone have grown from approximately 1/2 million gallons in 1999 to 250 million gallons in 2006, with continued growth expected [16]. Because every 10 pounds of biodiesel

* Corresponding author. Fax: +1 434 982 2658
E-mail address: rjd4f@virginia.edu (R.J. Davis).

0021-9517/$ – see front matter © 2007 Elsevier Inc. All rights reserved.
doi:10.1016/j.jcat.2007.06.001

produces about 1 pound of glycerol, the glycerol market is experiencing a surplus [17].

Investigations of glycerol oxidation over Au catalysts in the aqueous phase have reported a wide range of activities and selectivities, with most of the variations attributed to the influence of Au particle size [14,15,18,19]. The highest reported selectivity to the product glyceric acid was found over a 1 wt% Au/graphite catalyst with Au particle sizes of 5–50 nm, with most about 25 nm [18]. Others also have confirmed that larger Au particles (∼20 nm) result in increased selectivity to glyceric acid during glycerol oxidation [14,19]. However, smaller Au particle sizes apparently exhibited higher rates per surface Au atom compared with the larger particles [19]. In contrast to the studies mentioned above, Demirel-Gulen et al. observed that 3.7-nm Au particles were more selective to glyceric acid than both larger (23 and 42 nm) and smaller (2.7 nm) particles [15]. Evidently, there is no general consensus regarding the influence of Au particle size on glycerol oxidation catalysis.

We reported in a previous study that H_2O_2 is also formed during glycerol oxidation over gold catalysts and that the observed C–C cleavage that leads to glycolic acid formation is correlated with the presence of H_2O_2 [11]. Okumura et al. [20] observed that during the direct production of H_2O_2 from H_2 and O_2, large (30 nm) Au particles were inactive for H_2O_2 formation. We suspect that the selectivity patterns reported in the literature for glycerol oxidation over Au catalysts are directly the result of the H_2O_2 that is also produced in the reaction. In this work, a series of Au catalysts with a range of particle sizes was investigated in the oxidation of glycerol to glyceric and glycolic acid in the aqueous phase, with attention given to the production of peroxide. In addition, the aqueous-phase oxidation of CO was measured over the same Au catalysts in an attempt to generalize the oxidation results.

2. Experimental

2.1. Catalyst synthesis

A gold on carbon catalyst with a mean Au particle size of about 5 nm was prepared via the formation of a gold sol and subsequent deposition of the sol onto the catalyst support [21]. First, 0.15 g of $HAuCl_4{\cdot}3H_2O$ (∼50 wt% Au, Aldrich) was added to 3 L of distilled deionized water, followed by the addition of 0.075 g polyvinyl alcohol (PVA) (Acros). The gold colloid was subsequently reduced by the dropwise addition of 0.1 M $NaBH_4$ (Aldrich), using a 4:1 molar ratio of $NaBH_4$:Au. The resulting sol was ruby-red in color. Then 10 g of catalyst support, activated carbon (Calgon, type ADP), was suspended in 100 cm^3 of distilled deionized water and sonicated for 1 h before being added to the Au sol. The sol–carbon slurry was stirred for 1 h, at which point the catalyst was filtered. The filtrate had a slight red tint, indicating that not all of the Au sol had deposited onto the carbon support. The catalyst was then washed twice with 1 L of distilled deionized water to remove residual chlorine. The final filtrate tested negative for Cl^- using a 0.1 M $AgNO_3$ solution. The catalyst was then dried overnight in air at 403 K, reduced in N_2 and H_2 (90:10) flowing at 150 $cm^3\,min^{-1}$ by heating to 573 K at 4 $K\,min^{-1}$, held at 573 K for 6 h, and cooled to room temperature before being exposed to air. The catalyst was stored in a refrigerator at 278 K and used without any further pretreatment. The Au weight loading was determined by ICP (Galbraith Laboratories, Knoxville, TN). We designate this catalyst Au/Calgon.

Gold nanoparticles with a nominal diameter of 20 nm were synthesized by the citrate reduction method [22,23]. First, 2 cm^3 of a 25.4 mM $HAuCl_4$ solution ($AuCl_3$ 99.99%, Sigma–Aldrich) was diluted in 200 g of deionized water. The solution was stirred vigorously and heated until boiling. Next, 12 cm^3 of 34.5 mM trisodium citrate (>99.5%, Fisher) was added, and the solution was boiled for 30 min before cooling to room temperature. The final gold nanoparticle suspension had a reddish color.

Gold nanoparticles having a nominal diameter of 45 nm were synthesized by a two-step citrate reduction method in which 13-nm gold nanoparticles were first prepared and then used as seeds for the growth of 45-nm gold nanoparticles [24,25]. The 13-nm gold nanoparticles were synthesized by a method similar to that used to produce the 20-nm nanoparticles [26]. First, 2 cm^3 of 25.4 mM $HAuCl_4$ was diluted in 48 g of deionized water. The solution was stirred vigorously and heated until boiling. Then 5 cm^3 of 38.8 mM trisodium citrate was added, and the solution was boiled for 15 min before being removed from the heat source. Next, 125 cm^3 of a 0.296 mM $HAuCl_4$ solution was stirred vigorously and heated until boiling, at which time 1.125 cm^3 of the 13-nm gold nanoparticle suspension was added, followed by 0.56 ml of 38.8 mM trisodium citrate. The final solution was boiled for 30 min before cooling to room temperature. The 45-nm gold nanoparticle suspension had a dark-red color.

The 20-nm and 45-nm gold nanoparticles were then deposited onto carbon black (Fisher). This carbon support is different than the activated carbon described above. The amount of carbon black that would result in a 1 wt% Au catalyst was sonicated in 100 cm^3 of distilled deionized water and added to a Au nanoparticle suspension under vigorous stirring. The carbon-Au suspension was stirred for 1 h. The catalysts were then filtered and washed twice with 1 L of distilled deionized water. The final filtrates tested negative for Cl^- using a 0.1 M $AgNO_3$ solution. The samples were dried overnight in air at 403 K, reduced in N_2 and H_2 (90:10) flowing at 150 $cm^3\,min^{-1}$ by heating to 573 K at 4 $K\,min^{-1}$, held at 573 K for 6 h, and cooled to room temperature before being exposed to air. The catalysts were stored in a refrigerator at 278 K and used without any further pretreatment. The Au weight loading was determined by ICP (Galbraith Laboratories). The two catalysts prepared by this method are designated 20-nm Au and 45-nm Au, respectively.

A World Gold Council (WGC) reference catalyst, Au/C (type D, sample #20), was used as received. A data sheet accompanying the catalyst indicated that the Au/C was prepared by a gold sol method [27], and is designated Au/C. Gold powder spheres (>99.96%, Alfa Aesar) ranging in size from 500 to 800 nm were used as received and are designated Au powder. Silver powder spheres (99.9%, Alfa Aesar) ranging from 500 to 1000 nm were used as received and are designated Ag powder.

2.2. Transmission electron microscopy

Samples that were characterized by transmission electron microscopy (TEM) were first suspended in ethanol and agitated in an ultrasonic bath for 4 h. A drop of the suspended catalyst was applied to a copper mesh grid with lacey carbon film, and the ethanol was allowed to evaporate. TEM was performed on a JEOL 2010F transmission electron microscope operating at 200 kV and equipped with a Gatan imaging filter. All of the images were recorded using a slow-scan CCD camera and analyzed with the Gatan Digital Micrograph software package.

2.3. N_2 isotherms

N_2 physisorption was performed on a Micromeritics ASAP 2020 automated adsorption system. Before N_2 physisorption at 77 K, the samples were degassed at 573 K for 12 h. The BET method was used to evaluate the total surface area of the catalysts.

2.4. Oxidation reactions

The aqueous-phase CO oxidation reactions were performed in a 50-cm^3 batch reactor (Parr Instrument Company 4592). In the standard reaction, an appropriate amount of gold catalyst was added to 30 cm^3 of distilled deionized water. The reactor was then sealed and purged with He before the introduction of reactant gases (He 99.999%, CO 99.997%, and O_2 99.994%; Messer Gas). The feed gases were introduced to the reactor through a dip tube fitted with a 10-μm stainless steel frit. A stir bar and stir plate combination operating nominally at 1200 rpm was used for agitation. Gases were fed to the reactor via mass flow controllers, and the pressure (10 atm) was adjusted by a back-pressure regulator located on the exit line of the reactor. The total volumetric flowrate of CO, O_2, and He was 75 $cm^3\ min^{-1}$. Helium was used as an inert gas to keep the CO–O_2 mixture below the explosion limit. The effluent gases (CO, O_2, and CO_2) were analyzed by gas chomatography. For CO oxidation reactions operating at elevated pH, the product CO_2 was captured in the reaction solution as Na_2CO_3 and analyzed by liquid chomatography. Conversion of the limiting reactant was kept below 10% in all reactions.

The aqueous-phase oxidation of glycerol was performed in the same 50-cm^3 batch reactor. The glycerol (Acros) and NaOH (Mallinckrodt) were first dissolved in 30 cm^3 of distilled deionized water and then degassed with He before addition of the catalyst. The reactor was then sealed, purged with He, and heated to the desired reaction temperature before pressurizing with O_2. The pressure was maintained at a constant value by continually feeding O_2. Samples were periodically removed via a sample diptube (without a frit). The samples from the reaction were filtered (0.2 μm) and then analyzed by a Thermo Separation Products (TSP) Spectra Systems AS1000 high-performance liquid chromatograph (HPLC) equipped with a TSP Spectra Systems P2000 pump and Waters Differential Refractometer Model R401. An Aminex HPX-87H column (Bio-Rad) operating at 328 K and a 5 mM H_2SO_4 mobile phase flowing at 0.6 $cm^3\ min^{-1}$ were used for product separation. The retention times and calibration curves for observed products were determined by injecting known concentrations. Any CO_2 that was produced in the reaction was converted to Na_2CO_3 in the basic solutions and also was quantified by HPLC.

Hydrogen peroxide formed in the reaction mixture was evaluated by a colorimetric method [28]. First, 1 cm^3 of a filtered reaction sample was acidified with 1 cm^3 of 0.5 M H_2SO_4, to which 0.1 cm^3 of $TiO(SO_4)$ (15 wt% in dilute H_2SO_4, Aldrich) was added. Absorbance was then measured at 405 nm on a Varian Cary 3E UV-VIS spectrometer. A calibration curve of absorption versus H_2O_2 concentration was prepared by diluting a standard mixture of 30 wt% H_2O_2 (Fisher). The lower limit of H_2O_2 detection was ∼0.005 mM.

3. Results and discussion

3.1. Catalyst characterization

The catalyst weight loadings and particle sizes are presented in Table 1. A bright-field TEM image of Au/Calgon (Fig. 1) shows that most of the particles are 2–10 nm in diameter. Measurement of 533 particles gave a mean diameter of 5.0 nm, with a surface average diameter ($\sum d^3 / \sum d^2$) of 7.3 nm. The Au/C, provided by the WGC, had a broad particle size distribution, 4–40 nm in diameter (Fig. 2). Measurement of 265 particles of the Au/C sample produced a mean diameter of 12.2 nm, with a surface average diameter of 18.8 nm. Dispersion estimates for the Au/Calgon and Au/C were calculated by inverting the surface average diameter in nm. The resulting dispersions were used to normalize the observed rates to the number of Au surface atoms.

Figs. 3 and 4 show bright-field images of the 20- and 45-nm Au catalysts, respectively. Measurement of 111 particles for the 20-nm Au indicated a narrow particle size distribution with a mean diameter of 18.1 nm and the surface average diameter of 18.8 nm. Measurement of 104 particles for the 45-nm Au revealed that the most of the particles were around 45 nm, but a few smaller particles were also present. We suspect that these were seed particles that did not grow. The mean particle size for the 45-nm Au catalyst was 41.8 nm, with a surface aver-

Table 1
Physical properties of the Au and Ag catalysts

Catalyst	Metal (wt%)	Mean diameter[a] (nm)	Surface avg. diameter[b] (nm)	Metal surface area per g metal ($m^2\ g_{metal}^{-1}$)
Au/Calgon	0.53	5.0	7.3	38[c]
Au/C	0.8	12.2	18.8	14[c]
20 nm Au	0.92	18.1	18.8	14[d]
45 nm Au	0.99	41.8	43.5	6.1[d]
Au powder	>99.96	–	–	0.75[e]
Ag powder	99.9	–	–	2.1[e]

[a] Number-weighted mean diameter.
[b] Surface avg. diameter ($\sum d^3 / \sum d^2$), used in calculating Au surface area.
[c] Surface areas calculated using 0.0875 nm^2 (surface atom)$^{-1}$, Ref. [29].
[d] Calculated by treating the Au particles as spheres having the surface avg. diameter listed.
[e] Determined by N_2 physisorption.

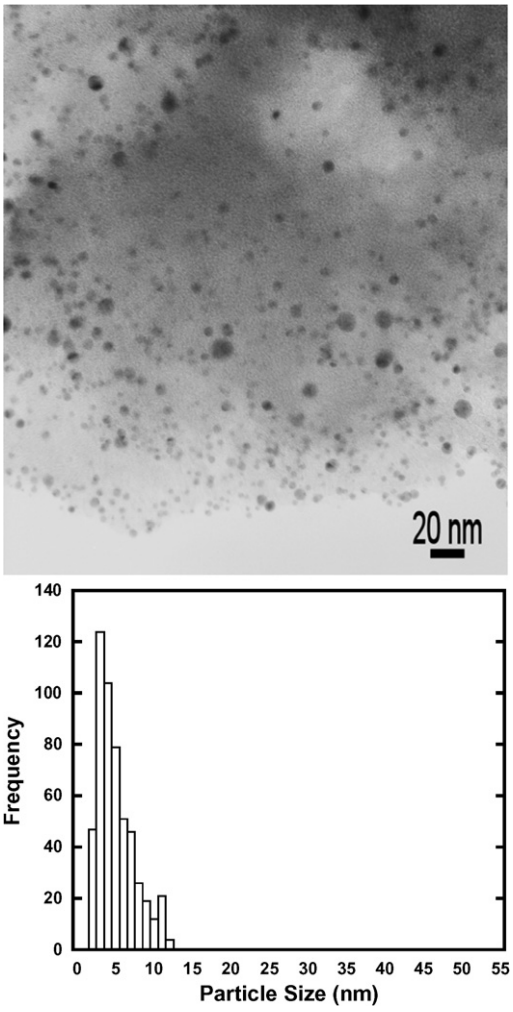

Fig. 1. Micrograph of Au/Calgon (top), with particle size distribution (bottom).

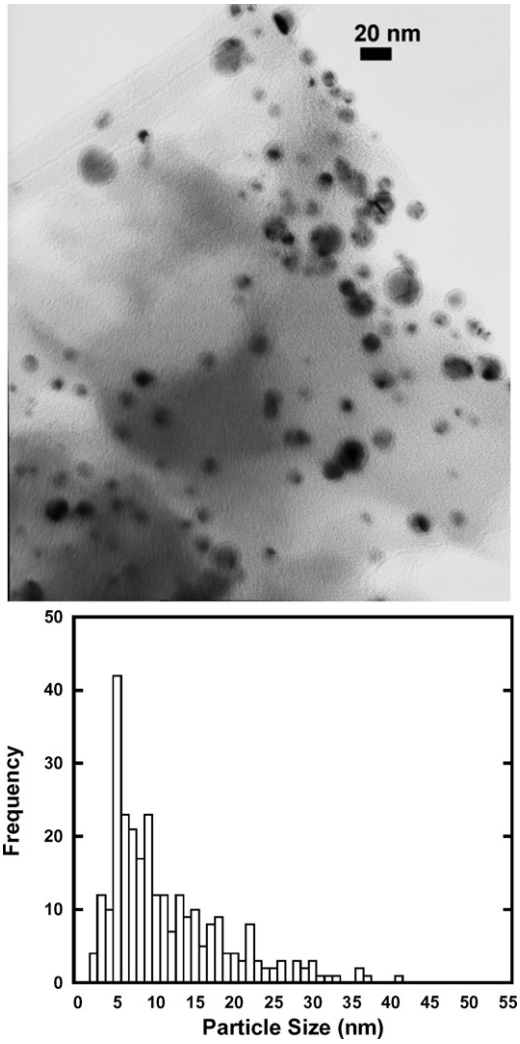

Fig. 2. Micrograph of Au/C (top), with particle size distribution (bottom).

age diameter of 43.5 nm. Surface areas for the 20- and 45-nm Au samples were determined by treating the particles as perfect spheres with the surface average diameter and a density of bulk Au. The number of exposed Au atoms was calculated from the geometric area assuming that 1 Au atom has an area of 0.0875 nm^2 [29]. The amount of Au atoms present at the surface was used to normalize the observed rate. Nitrogen physisorption was used to estimate the surface area of the Au and Ag powders. Assuming 0.0875 nm^2 (surface Au or Ag atom)$^{-1}$, the number of exposed Au and Ag atoms per gram of powder was determined. This calculation enabled us to estimate the observed reaction rates per exposed metal atom for the bulk materials.

3.2. Oxidation of CO

The Au/Calgon and Au/C samples were investigated previously by our group in both the vapor-phase and aqueous-phase oxidation of CO [11]. Although neither catalyst revealed activity in the vapor-phase oxidation of CO, both were quite active in the aqueous-phase oxidation. Table 2 shows how increasing the solution pH substantially increased the CO oxidation rate. Likewise, the rate of H_2O_2 production was enhanced by hydroxyl concentration. Both the Au/Calgon and Au/C samples had a significant fraction of particles with diameters of 5 nm or less. The 45-nm Au and Au powder were also tested for CO oxidation in the aqueous phase to determine whether large Au particles are also active for CO oxidation. As reported in Table 2, both the 45-nm Au and Au powder were active in aqueous-phase CO oxidation at neutral and basic pH. Although the TOFs of the 45-nm Au and Au powder were similar, they were an order of magnitude less than those of Au/Calgon and Au/C at elevated pH and two orders of magnitude less at neutral pH. These results support the idea that large Au particles are intrinsically less active than small Au particles, and also that the activity of large Au particles depends on pH to a greater extent than that of small Au particles. A similar trend of decreasing TOF with increasing particle size was observed by Kim et al. [9] over 1 wt% Au on carbon catalysts for the aqueous-phase oxidation of CO by polyoxometalates; however, it should be emphasized that bulk gold is active for oxidation reactions in the aqueous phase at high pH.

Of note, the purity of Au powders has been a concern in previous investigations of both CO oxidation and propylene oxidation [30,31], with Ag mentioned as the most abundant im-

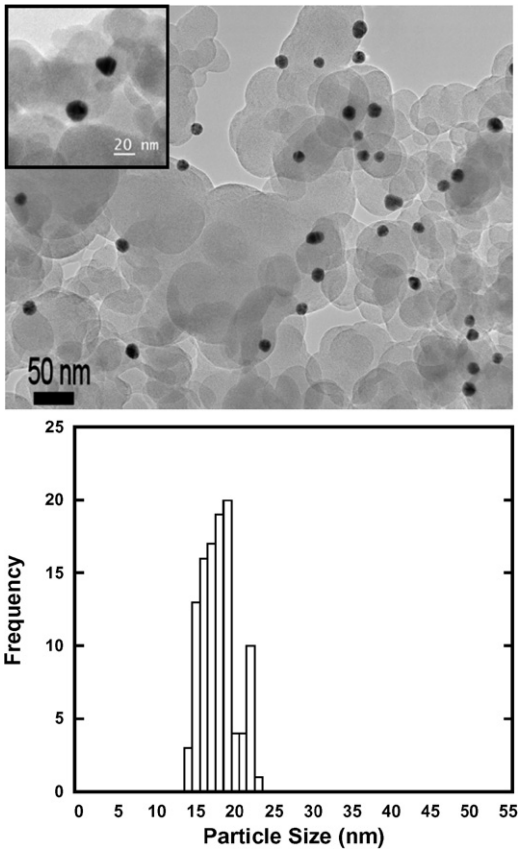

Fig. 3. Micrograph of carbon-supported 20 nm Au (top) with high-resolution micrograph (top, inset) and particle size distribution (bottom).

purity. Therefore, Ag powder was also tested for CO oxidation. The results, given in Table 2, show that Ag powder was inactive at both neutral and basic pH under our conditions of temperature and pressure. Therefore, if Ag was in fact an impurity on the Au powder surface, it did not contribute to the observed CO oxidation activity.

The similar TOF exhibited by Au/Calgon and Au/C for both CO oxidation and H_2O_2 formation is rather surprising given their different particle size distributions. Presumably, the Au/C should have lower TOF compared with Au/Calgon if a significant particle size effect exists, because Au/Calgon has smaller particles on average. Nevertheless, both samples have a significant number of particles smaller than 10 nm, with many smaller than 5 nm. Without explicit knowledge of how CO oxidation activity and H_2O_2 formation rate are affected by particle size, all we can conclude is that the rates are higher over catalysts with gold particles <10 nm in diameter. Larger particles exhibit rates equivalent to those observed on bulk gold. It is also important to note that different carbon supports were used for all three supported Au catalysts in this work.

Results from this work are consistent with those determined from the electrochemical oxidation of CO. Studies by Edens et al. [32] and Blizanac et al. [33] demonstrated activity for the electrochemical oxidation of CO over Au surfaces, with the observed rate depending on the exposed Au surface. However, both groups reported higher oxidation rates at elevated pH, with the formation of a hydroxycarbonyl suggested as the intermediate that leads to CO_2 [32,33]. A similar mechanism has been proposed by the Dumesic group for the oxidation of CO by aqueous-phase polyoxometalates over Au catalysts in the ab-

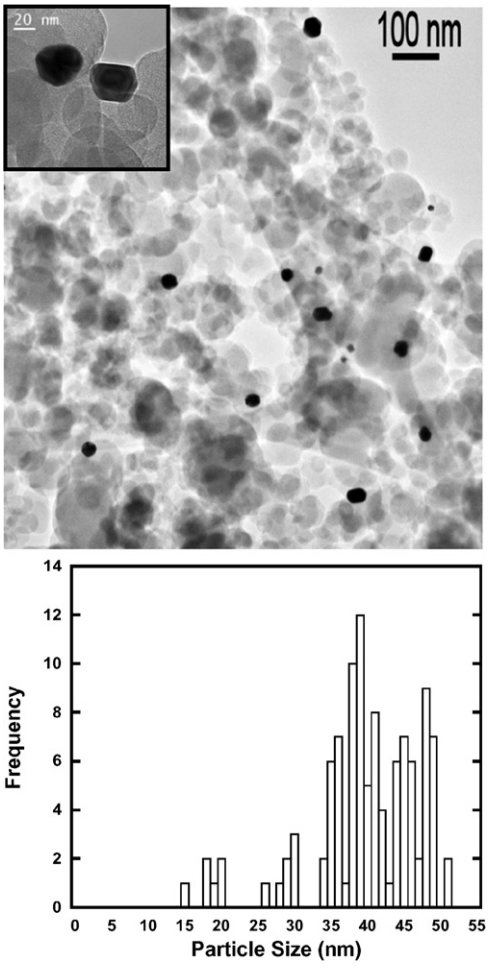

Fig. 4. Micrograph of carbon-supported 45 nm Au (top) with high-resolution micrograph (top, inset) and particle size distribution (bottom).

Table 2
Turnover frequency (TOF) for production of CO_2 and H_2O_2 at various pH values[a]

Catalyst	Product	TOF (s^{-1}) pH 0.3[c]	TOF (s^{-1}) pH 7	TOF (s^{-1}) pH 14[e]
Au/Calgon	CO_2	0.10	0.72	5.3
	H_2O_2[b]	b.d.[d]	0.03	0.54
Au/C	CO_2	0.12	0.47	5.4
	H_2O_2[b]	b.d.[d]	0.005	0.37
45 nm Au	CO_2	–	0.001	0.48
	H_2O_2[b]	–	b.d.[d]	0.01
Au powder	CO_2	b.d.[d]	0.003	0.36
	H_2O_2[b]	b.d.[d]	b.d.[d]	0.006
Ag powder	CO_2	–	b.d.[d]	b.d.[d]

[a] Reaction conditions, 10 atm, 300 K, 75 cm^3 min^{-1}; He:CO:O_2 (85:10:5).
[b] H_2O_2 rates determined following 1.5–2 h of reaction, not corrected for rate of decomposition.
[c] 0.5 M HNO_3.
[d] Below detection limits.
[e] 1 M NaOH, CO_2 measured by the formation of Na_2CO_3.

sence of an applied potential [10]. In their model, an adsorbed water molecule heterolytically dissociates (OH^- and H^+) on the gold surface. The adsorbed hydroxyl and adsorbed CO form the hydroxycarbonyl intermediate, which then leads to CO_2, with the net release of two protons into solution and two electrons transported though the metal to the polyoxometalate [10]. Similar TOFs were achieved when using O_2 instead of polyoxometalate as the oxidant [7], suggesting that a similar redox process was occurring. Thus, if hydroxycarbonyl is an intermediate during the aqueous-phase oxidation of CO by O_2, then a role of O_2 is to act as an electron scavenger on the Au. Indeed, the electrochemical reduction of O_2 to O_2^- on Au surfaces is enhanced at high pH [33–35]. After the formation of O_2^-, various routes can lead to the formation of hydrogen peroxide in the aqueous phase [36]. The fact that the H_2O_2 and CO_2 formation rates are influenced by pH, as reported in Table 2, supports this idea. It should be mentioned that hydroxycarbonyl has been proposed as a reaction intermediate in vapor-phase CO oxidation on supported Au particles [4].

3.3. Glycerol oxidation

A summary of the glycerol oxidation results is presented in Table 3 together with a representative reaction profile in Fig. 5. The concentrations and temperature used in this work (0.3 M glycerol, 0.6 M NaOH, 333 K) were typical of those used in previous studies [13–15]; however, only the Claus group used a dioxygen pressure of 10 atm. Because carbon-supported Au catalysts are generally considered more active than oxide-supported Au catalysts for glycerol oxidation [11,15,37], only carbon-supported materials were investigated here. To ensure that O_2 mass transfer was not limiting, the maximum O_2 transfer rate for our reactor configuration was determined by measuring the oxidation rate of an aqueous solution of Na_2SO_3 to Na_2SO_4 by O_2 [38]. The rate-controlling step in the reaction was assumed to be the mass transfer of O_2 from the vapor phase into the aqueous phase. The oxidation of sodium sulfite at our standard agitation speed and 10 atm O_2 resulted in a maximum transfer rate of 6×10^{-6} (mol O_2) s^{-1}. Therefore, catalyst loadings were selected to ensure that glycerol oxidation rates were below this value. The rates of glycerol consumption and H_2O_2 production given in Table 3 were based on the first 30 min of reaction. The rate of H_2O_2 production was not corrected for the decomposition reaction, that is, the rate was based on the observed amount of H_2O_2 at 30 min. Selectivity is defined as the total number of mol of species i formed per total number of mol of glycerol converted for the given reaction time. The molar sum of all C_3 and C_2 species was always within 3% of the initial glycerol loading in the reactor, which is within the expected error for HPLC analysis. The C_1 products consisted of carbon dioxide, trapped in solution as Na_2CO_3, and formic acid. Acids were present in their salt form at the elevated pH. A proposed reaction network accounting for all of the observed products has been presented previously [11].

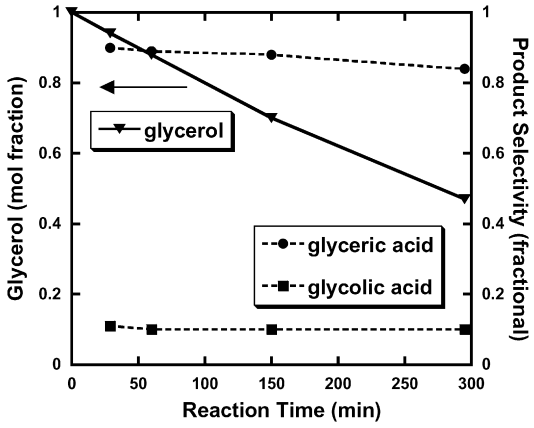

Fig. 5. Glycerol oxidation over carbon-supported 45 nm Au. Reaction conditions: 0.3 M glycerol, 0.6 M NaOH, glycerol:Au_s = 60,000:1, 333 K, O_2 = 10 atm.

The influence of O_2 pressure was investigated over Au/Calgon and bulk Au powder. In both cases, decreasing the O_2 pressure from 10 to 5 atm decreased the glycerol oxidation rate slightly but increased the peroxide formation rate. Although small changes in the glycerol oxidation products were observed, the lower O_2 pressure gave lower glyceric acid selectivities, presumably because of the higher peroxide levels.

Table 3
Rates of glycerol oxidation and H_2O_2 formation over Au and Ag catalysts[a]

Catalyst	Glycerol:Au_s (mol:mol)	O_2 press (atm)	Glycerol oxidation TOF (s^{-1})	H_2O_2[c] TOF (s^{-1})	S_{50} glyceric acid	S_{50} glycolic acid	S_{50} tartronic acid	S_{50} oxalic acid	S_{50} lactic acid
Au/calgon	110,000:1	10	17	0.34	0.64	0.29	0.03	0.01	0.03
Au/calgon	110,000:1	5	14	0.70	0.62	0.28	0.03	0.01	0.06
Au/calgon[b]	110,000:1	10	7.7	0.02	0.78[e]	0.19[e]	0.02[e]	0.01[e]	0.00[e]
Au/C	160,000:1	10	17	0.20	0.69	0.22	0.03	0.01	0.05
20 nm Au/C	60,000:1	10	2.3	0.11	0.78	0.16	0.02	0.00	0.04
45 nm Au/C	60,000:1	10	2.2	0.14	0.83	0.11	0.02	0.00	0.04
Au powder	60,000:1	10	2.5	0.18	0.80	0.16	0.01	0.00	0.03
Au powder	60,000:1	5	2.3	0.25	0.74	0.20	0.01	0.00	0.05
Ag powder	30,000:1	10	0.15	b.d.[d]	0.11	0.88	0.00	0.01	0.00

[a] Reaction conditions (30 cm^3, 0.3 M glycerol, 0.6 M NaOH, 333 K), product selectivity given at 50% conversion (S_{50}) for all observed C_3 and C_2 products.
[b] Standard reaction with the addition of 0.3 g MnO_2 (1.1 m^2 g^{-1}).
[c] H_2O_2 rates determined at t = 30 min, not corrected for rate of decomposition or consumption.
[d] Below detection limits.
[e] Selectivity given at 40% conversion.

Similar to the oxidation of CO in the aqueous phase, the TOFs for glycerol oxidation were about an order of magnitude higher for the Au/Calgon and Au/C catalysts compared with the samples with larger Au particles (Table 3). However, catalysts with larger Au particles had a higher selectivity to glyceric acid compared with Au/Calgon and Au/C. The 20-nm Au, 45-nm Au, and Au powder samples demonstrated similar activity and selectivity under the standard reaction conditions, suggesting that once the Au particle size reaches 20 nm, the Au particles function in the same manner as bulk Au. The observation that larger Au particles ($\geqslant$20 nm) are the most selective for glyceric acid formation agrees well with previous results [14,18].

To address the issue of the purity of Au powder during glycerol oxidation, the Ag powder was also tested under the standard reaction conditions. Table 3 reveals that Ag was active for glycerol oxidation but was an order of magnitude less active than Au powder. Moreover, the selectivity of the Ag catalyst favored glycolic acid instead of glyceric acid, the opposite of the Au catalysts. Therefore, any contribution of the observed rates over Au powder that might result from the presence of Ag surface impurities was neglected.

In previous work [11], we proposed that the observed C–C cleavage leading to the formation of glycolic acid can be attributed to the H_2O_2 formed in situ during glycerol oxidation over Au. To test this hypothesis, a known peroxide decomposer, MnO_2 [39], was added to the reaction mixture (see the third entry in Table 3). Approximately 0.3 g of MnO_2 (Aldrich), with a surface area of 1.1 $m^2\,g^{-1}$, was added to a standard glycerol oxidation reaction (30 cm^3, 0.3 M glycerol, 0.6 M NaOH, 333 K, 10 atm O_2, and Au/Calgon at glycerol:Au_s = 110,000:1). The initial concentration of H_2O_2 decreased from 1.7 mM H_2O_2 without MnO_2 to 0.12 mM with MnO_2, and the corresponding selectivity at 40% conversion increased from 64 to 78%. This confirmed the concept that peroxide formation is detrimental to glyceric acid formation over the Au/Calgon. However, addition of the MnO_2 decreased the initial glycerol oxidation activity of Au/Calgon by half, suggesting that some of the observed activity over Au catalysts may be due to the oxidizing ability of the peroxide or the peroxide precursor, superoxide.

From the previous test with MnO_2, it is clear that decreasing the concentration of H_2O_2 in solution will increase the selectivity of glycerol oxidation to glyceric acid. Inspection of Table 3 shows that the most active glycerol oxidation catalysts (Au/Calgon and Au/C) also had the highest peroxide formation rates. However, the glyceric acid selectivity over these catalysts at standard conditions (64–69%) was lower than that over the supported large particles or bulk gold (78–83%). Because a comprehensive peroxide decomposition study has not yet been performed over each catalyst, it is difficult to relate the observed H_2O_2 TOF to the observed selectivity during glycerol oxidation. Nevertheless, we observed peroxide formation over all of the Au particle sizes investigated, including bulk gold. Therefore, under the conditions investigated in this study, the formation of glycolic acid may be unavoidable over monometallic Au particles of any size.

During the electrochemical oxidation of glycerol over Au surfaces, Kahyaoglu et al. [40] and Avramov-Ivic et al. [41] observed that the glycerol oxidation rates increase with hydroxyl concentration, in agreement with our previously published results on supported Au catalysts [11]. For the catalytic oxidation of glucose over Au in the aqueous phase, Comotti et al. also reported an increase in the oxidation rate with hydroxyl concentration [42]. They also speculated that the hydrated glucose anion transfers an electron though the Au, which then reduces O_2 to O_2^- and eventually forms H_2O_2 [42]. These previous observations, together with our results from CO oxidation and glycerol oxidation, suggest that a complex redox process involving the Au catalyst, a reducing species (CO or glycerol), and an oxidizer (O_2) can account for the catalytic activity in the aqueous phase.

4. Conclusions

Investigation of carbon-supported Au catalysts for the aqueous-phase oxidation of CO revealed higher TOFs for catalysts composed of highly dispersed particles compared with those with large Au particles ($\geqslant$20 nm). Moreover, the reactivity of the larger Au particles had a greater dependence on the hydroxyl concentration in solution. The results indicate that hydroxyl adsorption on the Au surface is important for making Au catalysts that are inactive for the vapor-phase oxidation of CO very active in the aqueous phase.

During the aqueous-phase oxidation of glycerol, the same trend in activity with particle size was observed. The catalysts that were characterized by the presence of highly dispersed particles exhibited rates 7 times greater than catalysts containing particles of 20 nm or larger. Unsupported Au powder had similar rates and selectivities as those associated with monodispersed 20- and 45-nm supported Au particles. Evidently, 20-nm particles function the same as bulk Au.

The formation of peroxide during CO and glycerol oxidation in water suggests that peroxide formation is a general characteristic of Au-catalyzed oxidation. The formation of H_2O_2 during the glycerol oxidation reaction was observed over all of the Au catalysts, suggesting that the C–C cleavage product, glycolic acid, may be unavoidable over monometallic gold catalysts.

Acknowledgments

This work was supported by the National Science Foundation (grants CTS-0313484, CTS-0624608, EEC-0118007, and EEC-0647452) and a 3M Nontenured Faculty Award. Partial support also was provided from the U.S. Department of Energy, Office of Basic Energy Sciences (grant DE-FG02-95ER14549).

References

[1] A.S.K. Hashmi, G.J. Hutchings, Angew. Chem. Int. Ed. 45 (2006) 7896.
[2] G.C. Bond, C. Louis, D.T. Thompson, Catalysis by Gold, Imperial College Press, London, 2006.
[3] J.T. Calla, R.J. Davis, Ind. Eng. Chem. Res. 44 (2005) 5403.
[4] C.K. Costello, J.H. Yang, H.Y. Law, Y. Wang, J.N. Lin, L.D. Marks, M.C. Kung, H.H. Kung, Appl. Catal. A 243 (2003) 15.
[5] M. Date, M. Okumura, S. Tsubota, M. Haruta, Angew. Chem. Int. Ed. 43 (2004) 2129.

[6] M. Date, M. Haruta, J. Catal. 201 (2001) 221.
[7] M.A. Sanchez-Castillo, C. Couto, W.B. Kim, J.A. Dumesic, Angew. Chem. Int. Ed. 43 (2004) 1140.
[8] W.B. Kim, T. Voitl, G.J. Rodriquez-Rivera, J.A. Dumesic, Science 305 (2004) 1280.
[9] W.B. Kim, G.J. Rodriquez-Rivera, T. Voitl, S.T. Evans, J.J. Einspahr, P.M. Voyles, J.A. Dumesic, J. Catal. 235 (2005) 327.
[10] W.B. Kim, T. Voitl, G.J. Rodriquez-Rivera, S.T. Evans, J.A. Dumesic, Angew. Chem. Int. Ed. 44 (2005) 778.
[11] W.C. Ketchie, M. Murayama, R.J. Davis, Top. Catal. 44 (2007) 307.
[12] L. Prati, M. Rossi, J. Catal. 176 (1998) 552.
[13] S. Carrettin, P. McMorn, P. Johnston, K. Griffin, G.J. Hutchings, Chem. Commun. (2002) 696.
[14] F. Porta, L. Prati, J. Catal. 224 (2004) 397.
[15] S. Demirel-Gulen, M. Lucas, P. Claus, Catal. Today 102–103 (2005) 166.
[16] A.H. Tullo, C&E News 85 (2007) 53.
[17] M. McCoy, C&E News 84 (2006) 7.
[18] S. Carrettin, P. McMorn, P. Johnston, K. Griffin, C. Kiely, G.A. Attard, G.J. Hutchings, Top. Catal. 27 (2004) 131.
[19] N. Dimitratos, J.A. Lopez-Sanchez, D. Lennon, F. Porta, L. Prati, A. Villa, Catal. Lett. 108 (2006) 147.
[20] M. Okumura, Y. Kitagawa, K. Yamagcuhi, T. Akita, S. Tsubota, M. Haruta, Chem. Lett. 23 (2003) 822.
[21] L. Prati, G. Martra, Gold Bull. 32 (1999) 96.
[22] J. Turkevich, P. Stevenson, J. Hillier, Discuss. Faraday Soc. 11 (1951) 55.
[23] M.O. Nutt, J.B. Hughes, M.S. Wong, Environ. Sci. Technol. 39 (2005) 1346.
[24] S. Liu, M. Han, Adv. Func. Mat. 15 (2005) 961.
[25] C.D. Keating, K.K. Kovaleski, M.J. Natan, J. Phys. Chem. B 102 (1998) 9414.
[26] K.C. Graber, R.G. Freeman, M.B. Hommer, M. Natan, Anal. Chem. 67 (1995) 735.
[27] R. Holliday, Data sheets accompanying gold reference catalyst.
[28] C.N. Satterfield, A.H. Bonnell, Anal. Chem. 27 (1955) 1174.
[29] G. Bergeret, P. Gallezot, in: G. Ertl, H. Knoezinger, J. Weitkamp (Eds.), Handbook of Heterogeneous Catalysis, vol. 2, VCH, Weinheim, 1997, p. 441.
[30] Y. Iizuka, A. Kawamoto, K. Akita, M. Date, S. Tsubota, M. Okumura, M. Haruta, Catal. Lett. 97 (2004) 203.
[31] E.E. Stangland, K.B. Stavens, R.P. Andres, W.N. Delgass, J. Catal. 191 (2000) 332.
[32] G.J. Edens, A. Hamelin, M.J. Weaver, J. Phys. Chem. 100 (1996) 2322.
[33] B.B. Blizanac, C.A. Lucas, M.E. Gallagher, M. Arenz, P.N. Ross, N.M. Markovic, J. Phys. Chem. B 108 (2004) 625.
[34] S. Strbac, R.R. Adzic, J. Electroanal. Chem. 403 (1996) 169.
[35] M.H. Shao, R.R. Adzic, J. Phys. Chem. B 109 (2005) 16563.
[36] D.T. Sawyer, Oxygen Chemistry, vol. 1, Oxford Univ. Press, New York, 1991.
[37] N. Dimitratos, A. Villa, C.L. Bianchi, L. Prati, M. Makkee, Appl. Catal. A 311 (2006) 185.
[38] B. Maier, C. Dietrich, J. Buchs, Trans. IChemE. 79 (2001) 107.
[39] M.A. Hasan, M.I. Zaki, L. Pasupulety, K. Kumari, Appl. Catal. A 181 (1991) 171.
[40] A. Kahyaoglu, B. Beden, C. Lamy, Electrochim. Acta 29 (1984) 1489.
[41] M.L. Avramov-Ivic, J.M. Leger, C. Lamy, V.D. Jovic, S.D. Petrovic, J. Electroanal. Chem. 308 (1991) 309.
[42] M. Comotti, C.D. Pina, E. Falletta, M. Rossi, Adv. Syn. Catal. 348 (2006) 313.